Journal of Sol-Gel Science and Technology (2021) 100:477–488
https://doi.org/10.1007/s10971-021-05665-0

ORIGINAL PAPER: NANO- AND MACROPOROUS MATERIALS (AEROGELS, XEROGELS, CRYOGELS, ETC.)

Effects of precursor concentration on the physicochemical properties of ambient-pressure-dried MTES based aerogels with using pure water as the only solvent

Xi Deng[1] · Liling Wu[1] · Yunmeng Deng[1] · Siqi Huang[1] · Mengtian Sun[1] · Xiaowu Wang[1] · Qiong Liu[1] · Ming Li[1] · Zhi Li[1]

Received: 23 May 2021 / Accepted: 8 October 2021 / Published online: 9 November 2021

Abstract

This work presents a facile synthesis approach of methyltriethoxysilane (MTES) based aerogels using pure water as the only solvent, and the effects of precursor concentration on the physicochemical properties are investigated in detail. Therein, the precursor concentration has no effect on the chemical composition but causes the denser and slenderer skeletons at the lower precursor concentration and vice versa. At the 14.4 vol% precursor concentration, the MTES based aerogels are made up of slender skeletons, having the minimum density (0.057 g/cm^3), the maximum porosity (97.5%), and the low thermal conductivity (29.4 mW/m/K). It further finds the denser and slenderer silica skeletons cause higher compressive strength and higher Young's modulus. The TG-DSC results indicate the nice thermal stability of MTES based aerogels. In short, this research demonstrates the great competitive advantages of MTES based aerogels in the field of thermal insulation from the view of preparation method, thermal conductivity, and thermal stability.

Graphical Abstract

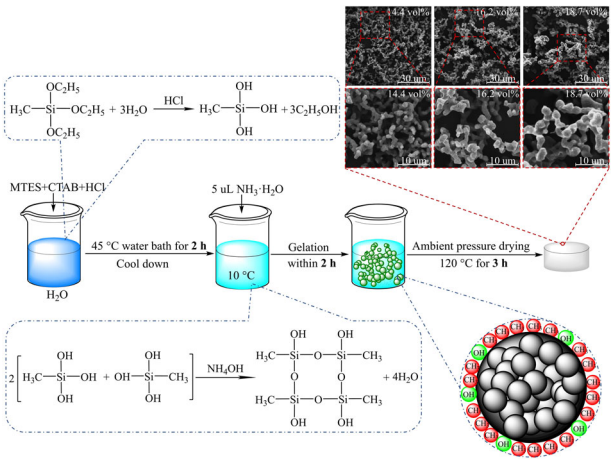

Keywords MTES based aerogel · Ambient pressure drying · Hydrophobicity · Thermal properties · Mechanical properties

✉ Ming Li
liming_csu@csu.edu.cn

✉ Zhi Li
lizhi89@csu.edu.cn

[1] School of Resource and Safety Engineering, Central South University, Changsha 410083, P. R. China

1 Introduction

Currently, the most common silica aerogels are made from the precursors like sodium silicate [1, 2] and tetrafunctional silicon alkoxides, usually tetraethoxysilane (TEOS) [3–5] or tetramethoxysilane (TMOS) [6]. After forming wet gels from these precursors, further surface modification is carried out by grafting organic groups onto silica skeletons, which changes the hydrophilic silica skeletons into hydrophobic ones. The introduced organic groups can prevent the silica skeletons from shrinkage to some extent, because of the so-called "spring back" effect [7, 8]. The commonly used modification agents are organic chlorosilane, such as trimethylchlorosilane (TMCS) [9], dimethyldichlorosilane (DMDCS) [4], and methyltrichlorosilane (MTCS) [10], which are costly and corrosive, not friendly to the equipment.

On the aspect of drying technology, substituting ambient pressure drying for CO_2 supercritical drying has been tried out [11]. However, an outstanding problem of ambient-pressure-drying technology is the severe damage of the pore structure derived from the capillary pressure [12], which results in a large volume shrinkage of silica aerogels as well as the dramatically increasing density and thermal conductivity. Furthermore, it is also not easy to synthesize monolithic aerogels by ambient pressure drying due to the crack of the silica network induced by the capillary pressure, though it can be achieved by optimizing the aging and solvent exchange process [3].

Considering the tedious and complex preparation process as well as the large consumption of organic solvents [12], a lot of researchers focus on simplifying the preparation process and reducing the preparation costs [13, 14]. For instance, some researchers have tried to synthesize silica aerogels using the precursors with inherent hydrophobic groups, such as methyltrimethoxysilane (MTMS) [15–17]. In this strategy, the excellent hydrophobicity is acquired without further surface modification. Nevertheless, the prolonged aging process and the solvent exchange are still inevitable, in which the unsafe methanol (MeOH) is usually used as a solvent [18, 19]. Some researchers have tried to synthesize MTMS based aerogel by using ethanol (EtOH) as the solvent to avoid using MeOH [20], though a little MeOH is still generated during the hydrolysis of MTMS.

Currently, MTES has been reported as the precursor for the preparation of silica aerogels [21–23], which has a similar molecular structure to MTMS but without the production of MeOH. However, using pure water as the only solvent to prepare ambient pressure dried MTES based aerogels [24, 25] is rarely reported. For the perspective of industrial preparation, using pure water as the only solvent can reduce the usage of organic solvent and sequentially reduce the preparation costs. Besides, the large organic solvent usage means a higher thermal hazard risk during the preparation process. Considering these two aspects, adopting MTES as the precursor and using pure water as the only solvent are a meaningful attempt for the expansion of preparation technologies of silica aerogels.

In this study, using pure water as the only solvent and MTES as the precursor, monolithic MTES based aerogels were synthesized under ambient pressure drying. It is found that the precursor concentrations have great effects on the preparation and physicochemical properties of MTES based aerogels. Here, the effects of precursor concentration on the physicochemical properties of MTES based aerogel are investigated in detail, including the microstructure and morphology, density and porosity, hydrophobicity, thermal and mechanical properties. The outcomes provide a new example to develop the rapid and cost-effective preparation of high-quality MTES based aerogels for their practical applications.

2 Experimental methodology

2.1 Materials and preparation

Methyltriethoxysilane (MTES, 98%), cetyltrimethylammonium bromide (CTAB, 99%) from Aladdin (USA) were used as the precursor and cationic surfactant respectively. Ultrapure water (DI·H2O) produced by HHitech (China) Eco-S15UVFV acted as the only solvent. Hydrochloric acid (36–38%, HCl) and ammonium hydroxide (25–28%, $NH_3{\cdot}H_2O$) of CP grade from Sinopharm Chemical Reagent Co. Ltd. (SCRC, China) were used as acid and base catalytic agents, respectively. All these chemicals were used as received without further purification.

Firstly, 5 mL MTES, 0.01 g CTAB (based on the preliminary experiment as discussed as follow), and 300 uL 0.1 M HCl are mixed in DI·H2O in a 100 mL beaker with stirring for 3 min. DI·H2O was set as a series of volumes from 21 to 29 mL to change the precursor concentration. The obtained hybrid solution was kept in a 45 °C water bath and stirred to hydrolyze for about 2 h. Note that too fast condensation speed leads to the precipitation of silica skeletons instead of the gelation. Here, the hybrid solution was cooled to below 10 °C to adjust the condensation rate according to the Arrhenius equation [26], which aims to ensure the monolithic sample can be obtained in examined precursor concentration range and improve the physical properties simultaneously. Within stirring in 10 s, 1 M $NH_3{\cdot}H_2O$ of 500 uL was added into the hybrid solution. Subsequently, the formed sol was placed in an incubator below 10 °C and the gelation usually occurred within 1.5 h. At last, the wet gel was dried under ambient pressure at 120 °C for 3 h to obtain MTES based aerogel monoliths.

2.2 Characterization

The bulk density was calculated by measuring the mass and volume of pie samples, and the porosity was calculated as followed [3]:

$$Porosity\% = \left(1 - \frac{\rho_b}{\rho_s}\right) \times 100\% \quad (1)$$

where ρ_b and ρ_s represent the bulk density and skeletal density respectively. For silica aerogels, ρ_s is 2.25 g/cm^3 [27].

The microstructure of MTES based aerogels was observed by a field emission scanning electron microscope (SEM, JEOL JSM-7900F, Japan). Nitrogen adsorption-desorption isotherms were measured at 77 K using a surface characterization analyzer (Quantachrome AUTOSORB IQ, USA) after a prior degassing step of 8 h at 100 °C. The pore size distributions and cumulative pore volume were calculated using the BJH (Barrett-Joyner-Halenda) method [28]. The solvent surface tension was tested by the automatic surface tension meter (QBZY series, Shanghai Fangrui Instrument Co. Ltd.) at room temperature. The hydrophobicity was tested by a contact angle instrument (JC2000D1, Shanghai Zhongchen Instrument Co., Ltd., China), in which a 5 µL water droplet was dropped on the sample surface, and the contact angle was recorded and acquired by the imaging processing program, ImageJ [29]. The chemical bonds were studied by Fourier transform infrared spectra (FTIR, Thermo Nicolet iS50, USA) with MTES based aerogel powder in KBr pellet. The thermal conductivity was tested by a thermal conductivity meter (XIATECH, TC3000E probe, China) at room temperature and ambient pressure. To analysis the thermal stability, the thermogravimetry analyzer coupled differential scanning calorimeter (TG-DSC, Waters Corporation SDT 650, USA) was employed under the heating rate of 10 °C/min from room temperature up to 1000 °C in the air atmosphere. The mechanical properties were characterized by the uniaxial compression test (MTS Insight, USA) under the loading rate of 0.5 mm/min.

3 Results and discussion

3.1 Microstructure

The microstructures of samples with different precursor concentrations are compared in Fig. 1, in which the skeletons of MTES based aerogels are composed of coralloid branches. With the precursor concentration rising from 14.4 to 18.7 vol%, the silica skeletons become thick and sparse in Fig. 1a–c, and the average diameter of the silica skeletons also increases from ~1.3 µm to ~1.8 µm. The lower precursor concentration generates a more dispersed distribution of secondary particles in the crosslinking silica skeletons, which results in the formation of the slender backbone.

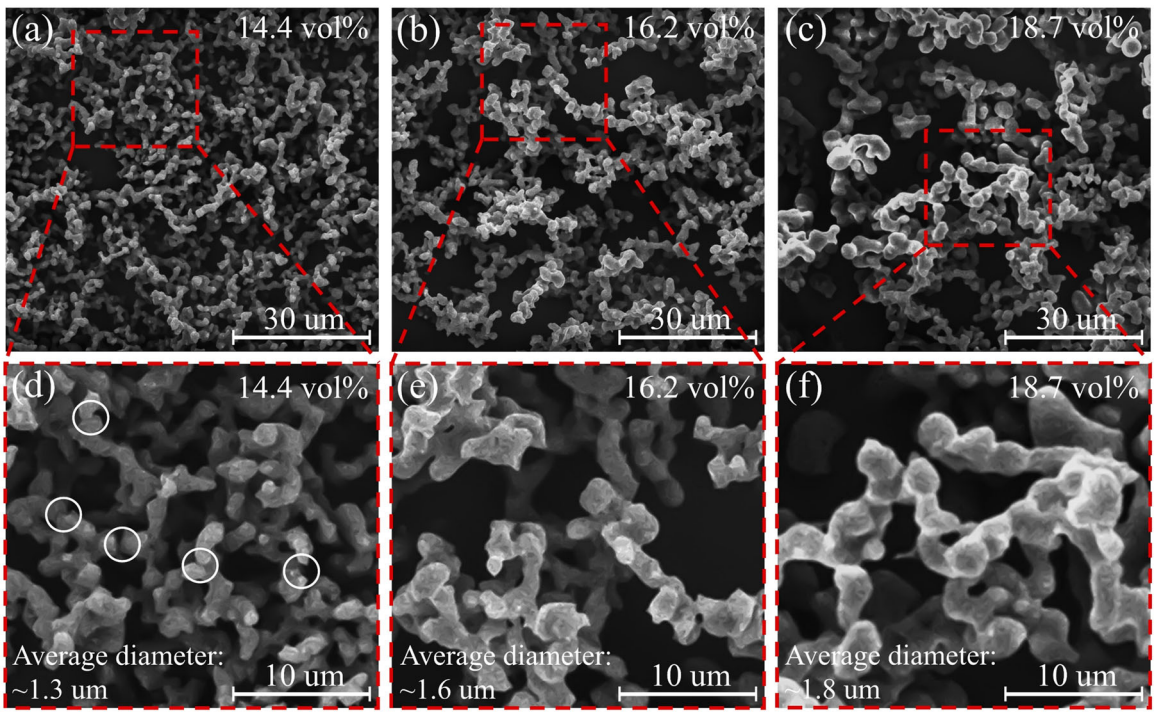

Fig. 1 SEM images of samples with different precursor concentrations, (**a**, **d**) 14.4 vol%, (**b**, **e**) 16.2 vol% and (**c**, **f**) 18.7 vol%, respectively

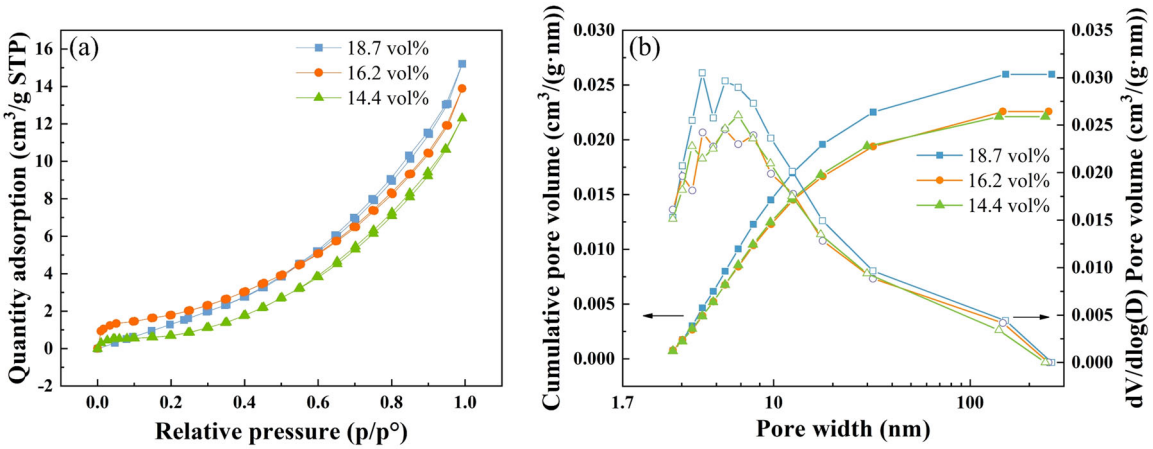

Fig. 2 **a** N_2 adsorption-desorption isotherms and (**b**) distributions of cumulative pore volume (solid symbols) and differential pore volume dV/dlog (D) (hollow symbols) by BJH method based on the N_2 adsorption branch for the MTES based aerogels with various precursor concentrations

As the precursor concentration increases, sufficient hydrolyzed MTES in the solvent promote the continuous growth of the skeletons through the condensation reaction. Besides, some formed secondary particles also attach to these skeletons through a dissolution-reprecipitation process [30]. As a consequence, the thick silica skeletons for the higher precursor concentration are formed as shown in Fig. 1c.

To further investigate the pore structure of MTES based aerogels, the nitrogen adsorption-desorption isotherms of the MTES based aerogels prepared with different precursor concentrations were measured. In Fig. 2a, all the MTES based aerogels have similar nitrogen isotherms and pore size distribution. To be specific, the adsorption quantities are low and the nitrogen adsorption-desorption isotherms belong to type II [31], which indicate the macropores and micron-sized pores (as shown in Fig. 1) in MTES based aerogels. Further, the hysteresis loops correspond to the type H3, suggesting the existence of slit-like interparticle pores [32]. Thereinto, the MTES based aerogel with 18.7 vol% precursor concentration shows higher adsorption quantity and mesopore volume. Because the higher precursor concentration causes the thicker silica skeletons, which contain more mesopores and micropores. Note that the N_2 adsorption-desorption test only partially reveals the pore structure with the pore size from 1.7 to 300 nm [19]. For further acquiring more details about the pore parameters of the MTES based aerogels, we calculate the total pore volume (V_{total}) and the average pore size of all the pores (D_{pore}) as following equations [33], which have been presented in Table 1.

$$D_{pore} = 4V_{total}/S_{BET} \quad (2)$$

$$V_{total} = 1/\rho_b - 1/\rho_s \quad (3)$$

where S_{BET} is the BET surface area. It finds that the surface area and total pore volume both decrease with the precursor concentration increasing, while the average pore size rises up significantly. These variations are exactly consistent with the SEM results in Fig. 1.

Table 1 The physical properties of MTES based aerogels with different precursor concentration

Precursor concentration	18.7 vol%	16.2 vol%	14.4 vol%
V_{total} (cm^3/g)	13.96	15.92	16.99
S_{BET} (m^2/g)	2.75	6.68	11.71
D_{pore} (um)	24.71	9.54	4.77

As discussed above, most of the pores in MTES based aerogels are micron-scale, but some micropores and mesopores still exist on the skeletons, such as in the secondary particles. The capillary tension inevitably causes the collapse of some silica skeletons during ambient pressure drying. In Fig. 1d, the fractures induced by those collapses have been marked with circles. It finds that more fractures are observed on the silica skeletons of the MTES based aerogel prepared with the lower precursor concentration. This result is just consistent with the characteristics of the slender but weak backbones of the samples at a lower precursor concentration. Furthermore, these produced fractures also act as the defects to influence the morphology and physicochemical properties, which will be discussed in the following contents.

3.2 Morphology, density, and porosity

As we know, the solvent surface tension has a great influence on the ambient pressure drying process, hence the solvent surface tension with various CTAB contents are tested in this section. In Fig. 3a, the CTAB has a significant effect on reducing the surface tension of DI·H_2O. Compared to pure DI·H_2O (71.4 mN/m), the solvent surface tension is reduced to 35.1 mN/m when the CTAB content is 0.005 g. However, phase separation occurs (Fig. 3b) in this case.

Because this amount of CTAB is too less to suppress the strong hydrophobicity of methylsiloxane network [34], rendering the hydrolyzed MTES precursor and water separate from each other. With the CTAB content increasing between 0.01 and 0.04 g, the solvent surface tension vibrates around 30.0 mN/m. And it finds the cylindrical (Fig. 3c) and caky (Fig. 3d) samples can be obtained merely at the CTAB content of 0.01 g. The samples begin to crack and the volume shrinkage increases significantly with the CTAB rising to over 0.01 g, as shown in Fig. 3e–g.

From the above analysis, the effect of CTAB content on solvent surface tension is minor when the CTAB content exceeding 0.01 g, hence the cracks of the samples should be induced by other reasons. Actually, the excessive CTAB acts as obstacles among the reactive species in the condensation reaction, which impede or reduce the crosslinking among the hydrolyzed MTES precursors. That further results in the formation of weaker silica skeletons, smaller secondary particles, and pores [35]. As we know, the weaker silica network is hard to resist the capillary force during the ambient pressure drying, hence the cracks are finally generated on these samples (Fig. 3e–g).

On the aspects of density and porosity, the bulk density increases from 0.057 g/cm^3 to 0.069 g/cm^3 with the precursor concentration increasing from 14.4 to 18.7 vol% in Fig. 4a. The weight fraction of precursor concentration and SiO_2 concentration are given in Table 2, the SiO_2 is the main component of obtained aerogel, hence the bulk density shows an increasing tendency with the SiO_2 concentration increase from 4.3 to 5.6 wt%. During the condensation reaction, the lower precursor concentration results in more dispersed secondary particles, which further causes to form the slender silica skeletons. As a consequence, the smaller density of MTES based aerogels is obtained at a lower precursor concentration; vice versa. As it is known to us, the porosity has an opposite trend to the density, which is determined by Eq. (1). Despite decreasing from 97.5 to 96.9%, the high porosity is still maintained.

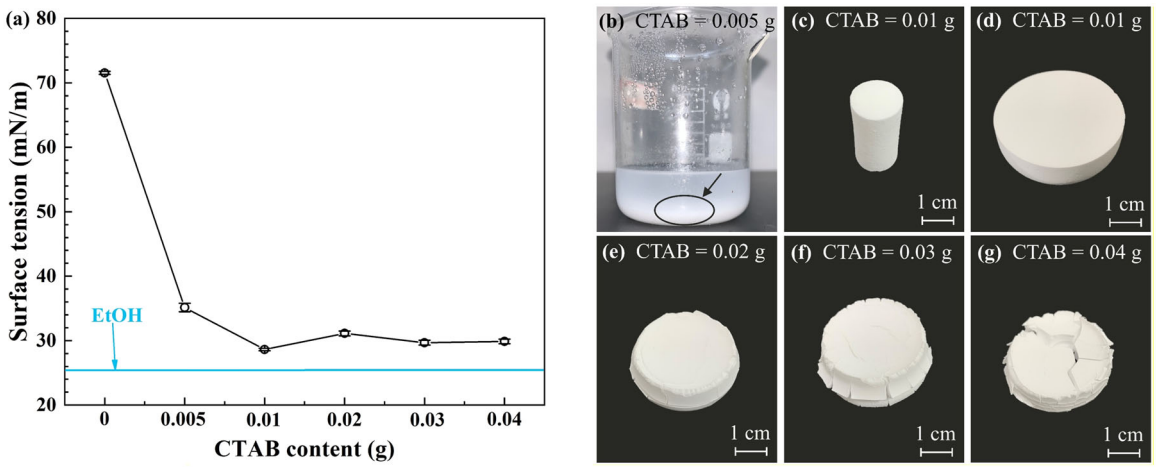

Fig. 3 **a** The surface tension of water with different CTAB contents. Samples with various CTAB content, (**b**) CTAB = 0.005 g, (**c**, **d**) CTAB = 0.01 g, (**e**) CTAB = 0.02 g, (**f**) CTAB = 0.03 g and (**g**) CTAB = 0.04 g

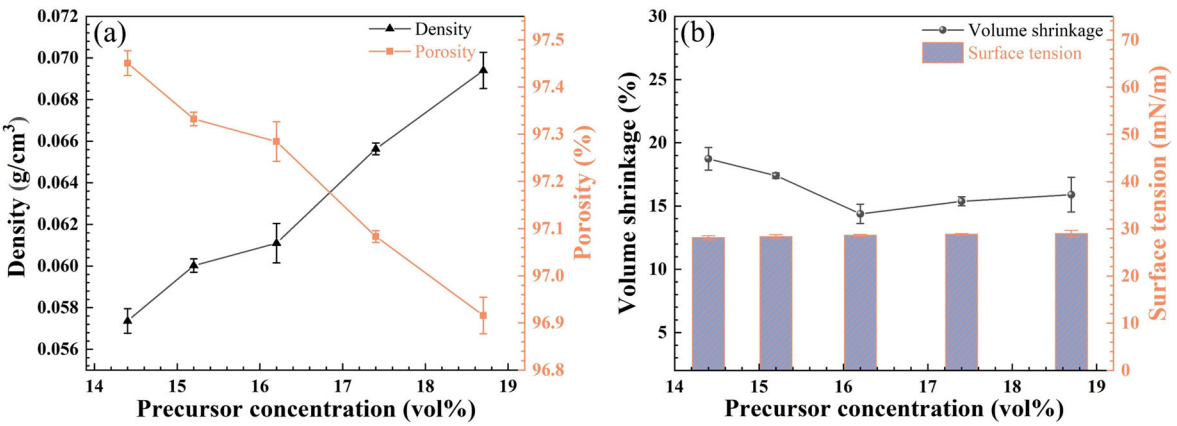

Fig. 4 **a** The variation of density, porosity, and (**b**) the volume shrinkage and the solvent surface tension of various precursor concentrations

In Fig. 4b, the volume shrinkage ranges from 15.8 to 18.8%. As stated above, the lower precursor concentration forms the slender silica skeletons, which are easily destroyed by the capillary force during the ambient pressure drying [18], for example, the sample presented in Fig. 1d. Finally, a relatively higher volume shrinkage is obtained. With the precursor concentration increasing to 16.2 vol%, the generated silica skeletons are strong enough to resistant to the capillary force, which leads to the lowest volume shrinkage. When the precursor concentration continues to increase, that effect is not obvious anymore; on the contrary, the volume shrinkage rises slightly [27, 34]. Besides, the solvent surface tensions have few distinctions in each as shown in Fig. 4b, hence the difference of capillary force can be neglected. As discussed above, there are more fractures on the silica skeleton of lower precursor concentration sample, which is the main reason for volume shrinkage in this work. To sum up, the change of volume shrinkage is not significant, and it mainly depends on the precursor concentration instead of solvent surface tension.

3.3 Hydrophobicity and FTIR

During the synthetic process, the hydrolysis and condensation reactions in this study are presented in the following equations [22]. Therein, the Si–CH_3 groups are kept on the hydrolyzed MTES molecules and the oligomers all the time. These non-hydrolytic Si–CH_3 groups finally are transferred to the silica skeletons and play an essential role in determining the surface chemistry properties of MTES based aerogels [33].

Hydrolysis:

(4)

Condensation:

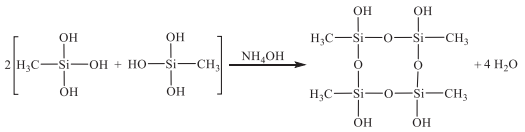

(5)

As we know, the hydrophobicity of materials depends on their surface chemical composition and surface roughness [36]. Usually, hydrophobicity is characterized by the water contact angle. As shown in Fig. 5a, the water drop stands stably on the MTES based aerogel surface and the contact angle of 151° is obtained through the image analysis by the ImageJ software [29]. Although the precursor concentrations are different, all the prepared samples have a contact angle of over 150°. From the perspective of the contact angle, the precursor concentrations have no significant influence on the hydrophobicity of MTES based aerogels.

Figure 5b clearly shows the FTIR spectrums of MTES based aerogels prepared with various precursor concentrations. For silica aerogels, typical bands of Si–O–Si bonds asymmetric stretching vibration located in 1010–1090 cm^{-1} are present [37, 38]. The broader peaks at 3436 cm^{-1} and

Table 2 Precursor concentration in the forms of volume fraction, weight fraction, and SiO_2 weight fraction

Expressed way	Precursor concentration or SiO_2 concentration				
Vol%	14.4	15.2	16.2	17.4	18.7
Wt%	12.8	13.6	14.4	15.5	16.6
SiO_2 wt%	4.3	4.6	4.9	5.2	5.6

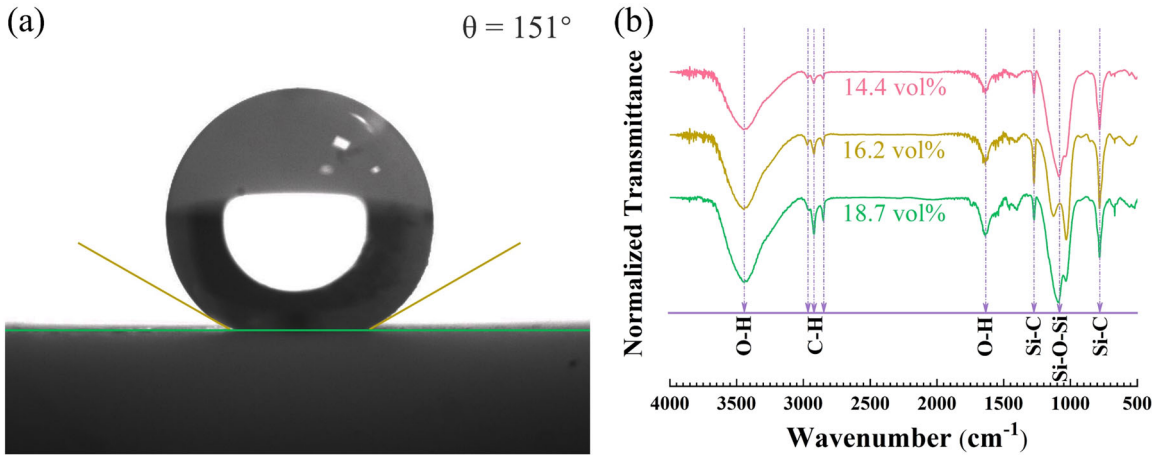

Fig. 5 (**a**) The contact angle of an MTES based aerogel sample and (**b**) the normalized FTIR spectrums of MTES based aerogels with various precursor concentrations

the peaks around 1647 cm^{-1} are ascribed to the –OH groups stretching vibration and deformation vibration respectively [39], which come from the unreacted hydrolyzed MTES precursors [40]. The peaks located at 782 and 1272 cm^{-1} are interpreted as stretching vibration and symmetric deformation vibration of Si–C bonds [37], which confirms the existence of hydrophobic groups ($Si–CH_3$) in MTES based aerogels [41]. And these hydrophobic $Si–CH_3$ groups are just the chemical foundation for the excellent hydrophobicity of MTES based aerogels. Three slight peaks at 2852, 2952, and 2971 cm^{-1} are caused by the asymmetric and symmetric stretching vibrations of C–H bonds [42]. These C–H bonds are mainly from the $Si–CH_3$ groups and a thimbleful of them are from the $Si–OC_2H_5$ groups, which are not involved in the hydrolysis reactions.

Furthermore, the intensity of the Si–C bond prepared with 16.2 vol% precursor concentration is the largest among the three spectrums. But the sample prepared with 18.7 vol % precursor concentration has a larger C–H intensity. It can be speculated that more unhydrolyzed $Si–OC_2H_5$ groups remain in the higher precursor concentration MTES based aerogels. To sum up, the precursor concentrations do not influence the chemical composition, but the intensity of Si–C, C–H, and Si–OH groups to some extent. That change further has a limited effect on hydrophobicity because of the simultaneous influence from the surface roughness [36].

3.4 Thermal conductivity

As it is reported [27], the MTMS or MTES based aerogels can be prepared rapidly without tedious solvent exchange and additional surface modification. Besides, the generated pores and silica skeletons in MTMS or MTES based aerogels are usually micron-sized [42]. As a result, the larger pores and thicker silica skeletons make the ambient pressure drying available for the preparation of MTMS or MTES based aerogels, though the capillary tension still exists.

Due to the micron-sized microstructure, the thermal conductivities of MTMS and MTES based aerogels usually range within 35–57 mW/m/K [30, 43], which is far larger than those of the TMOS, TEOS and sodium silicate based aerogels in Fig. 6. Here, we report that the thermal conductivity of the MTES based aerogels can reach as low as 29.4 mW/m/K at the precursor concentration of 14.4 vol%. Compared to the currently reported thermal conductivities of the ambient pressure dried MTMS and MTES based aerogels, the MTES based aerogels in this work has much lower thermal conductivity [27].

Here, we think the following reasons lead to the current low thermal conductivity. First, the silica skeletons in this study are coralloid, i.e., a more irregular skeletal structure, which produces larger thermal resistance. Second, the structural connectivity of coralloid skeletons is much worse than that of the reported spherical skeletons [27, 30]. The not-good connectivity increases the thermal resistance between the solid skeleton and gas phase, which impairs the heat transfer. In a word, the coralloid silica skeletons cause irregular skeletal structure and not-good connectivity, which further result in the increase of thermal resistance. Consequently, the relatively low thermal conductivity is obtained in this study.

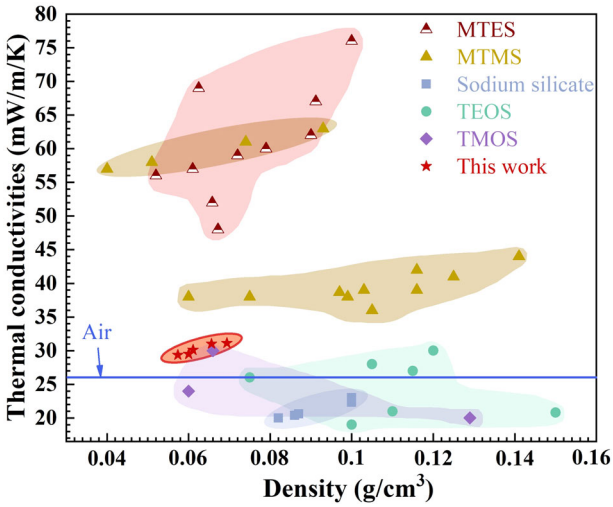

Fig. 6 Thermal conductivities with density of silica aerogels prepared with various precursors, including TMOS [59–61], TEOS [4, 62–64], sodium silicate [55, 65, 66], MTMS [27, 43, 67], and MTES [21, 24, 25]; the straight line is the thermal conductivity of still air

Considering the fast preparation process and water as the only solvent in this study, the prepared MTES based aerogel with the lower thermal conductivity significantly has a competitive advantage in the thermal insulation field, though this thermal conductivity is a little larger than the TEOS or sodium silicate based aerogels.

The effective thermal conductivity (λ_{eff}) of silica aerogel can be expressed as below [44]:

$$\lambda_{eff} = \lambda_s + \lambda_g + \lambda_r \tag{6}$$

where λ_s is the solid thermal conductivity of silica skeleton, λ_g is the thermal conductivity of the gaseous phase in the porous structure, and λ_r is the radiant thermal conductivity. Usually, the radiative thermal conductivity can be neglected under room temperature [45]. The solid thermal conductivity λ_s strongly depends on the density and silica skeleton morphology, which generally has a positive relationship with the density [46]. In regard of λ_g, it can be expressed as [47]:

$$\lambda_g = \frac{\lambda_{g0}}{1 + \alpha Kn} \tag{7}$$

$$Kn = \frac{l_m}{l_c} \tag{8}$$

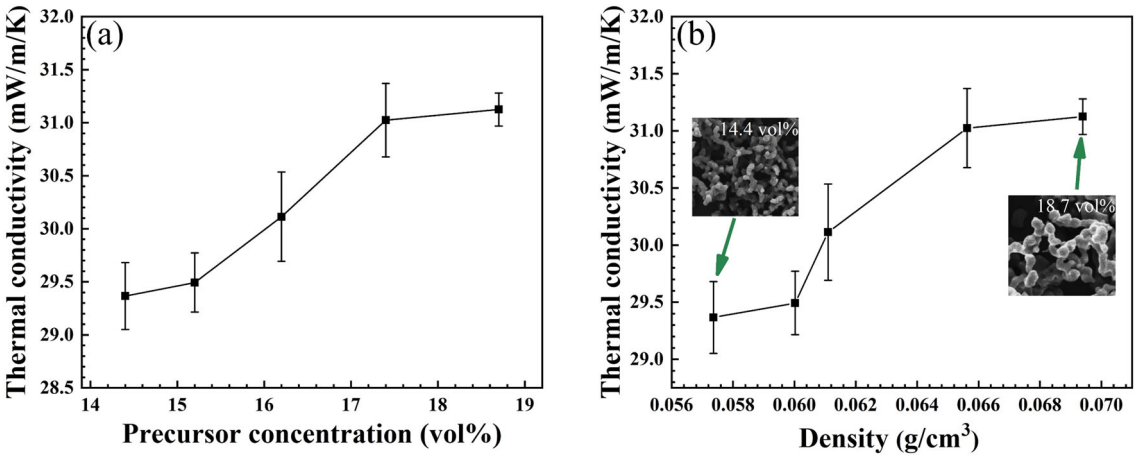

Fig. 7 The correlations of (**a**) the thermal conductivity versus the precursor concentration and (**b**) the thermal conductivity versus the density

where λ_{g0} is the thermal conductivity of air; α is a constant, related to the gas in the pores; K_n is the Knudsen number, which is determined by the ratio of the mean free path (l_m, nm, which is about 70 nm at 25 °C under atmospheric pressure) of air molecules in free air [46] and the average pore size of porous materials (l_c, nm) [47]. Obviously, with the rise of l_m or the decrease of l_c, the K_n increases, leading to a lower λ_g. In general, there are two options to reduce λ_g, i.e., evacuating the air in pores or decreasing the pore sizes [48].

Figure 7 presents the relationships among the thermal conductivity, precursor concentration, and density. At the precursor concentration below 17.4 vol%, the thermal conductivity increases rapidly and then keeps almost unchanged between the precursor concentration at 17.4–18.7 vol% in Fig. 7a. The tendency of thermal conductivity is considered to be related to the change of microstructure. As discussed above, the slenderer and denser three-dimensional silica network formed at a lower precursor concentration extends the path of heat conduction in the silica backbone [49]. Hence, the thermal resistance gets higher during the heat transfer process, leading to a lower solid thermal conductivity. With the precursor concentration rising, the silica skeletons become thicker and provide more heat transfer passages, which finally result in a higher solid thermal conductivity. Note that within the whole discussed precursor concentration range (14.4–18.7 vol%), the pore size is micron-sized, so the Knudsen effect almost has no influence on the heat transfer. Hence, the gaseous thermal conductivities (λg) are considered the same between each sample and the thermal conductivity mainly depends on the solid silica skeletons. Figure 7b displays the variation of thermal conductivity with the density, in which the thermal conductivity shows a positive correlation with the density. Because more solid silica skeletons mean more heat transfer passages. This result is just completely consistent with what analyzed before.

3.5 Thermal stability

As shown in Fig. 8a, the slight weight loss I in the temperature from 200 to 425 °C corresponds to the residual liquid, the remained unhydrolyzed Si–OC_2H_5 groups, and a very small amount of CTAB [50]. The obvious weight loss II occurs within the range of 425–560 °C, which is attributed to the thermal oxidation of Si–CH_3 groups on the silica skeletons of MTES based aerogels [39]. Furthermore, the significant peak on the DSC curve indicates that the thermal oxidation of Si–CH_3 groups is an exothermic reaction. Therein, the onset temperature (T_{onset}) and the peak temperature (T_{peak}) of the exothermic reaction are 425 and 510 °C, respectively. With the temperature rising continuously, the mass of MTES based aerogel keeps decreasing slightly before reaching 1000 °C, which should be primarily ascribed to the condensation among the newly generated Si–OH groups by the thermal oxidation [51].

As shown in Fig. 8b, the typical T_{onset} for TEOS and TMOS based aerogels are 261 and 287 °C, respectively [4, 52–54], while the sodium silicate based aerogels and MTMS based aerogels have a larger T_{onset} of 401 °C [55–57] and 432 °C [20, 27, 50], respectively. Based on our knowledge, the thermal stability of silica aerogels is mainly related to the microstructure, surface chemistry (i.e., surface organic groups), and component. Currently, our group has begun to devote to exploring the control mechanism of the thermal stability of silica aerogels [41]. In this work, the T_{onset} of as-prepared MTES based aerogels is 425 °C, the same with the MTMS based aerogels, which is even larger than the sodium silicate based silica aerogels. From the view of being the thermal insulation materials, the MTES based aerogels possess the higher thermal stability (425 °C), which presents an evident advantage.

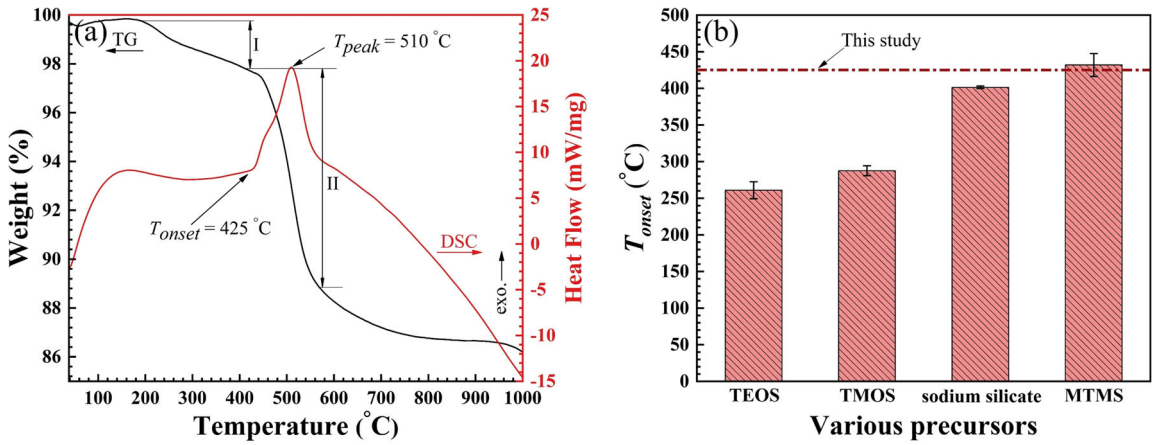

Fig. 8 **a** TG-DSC curves of MTES based aerogel under a heating rate of 10 °C/min in air atmosphere and (**b**) the onset temperatures of silica aerogels prepared with various precursors, the dash line is T_{onset} of MTES based aerogel in this study

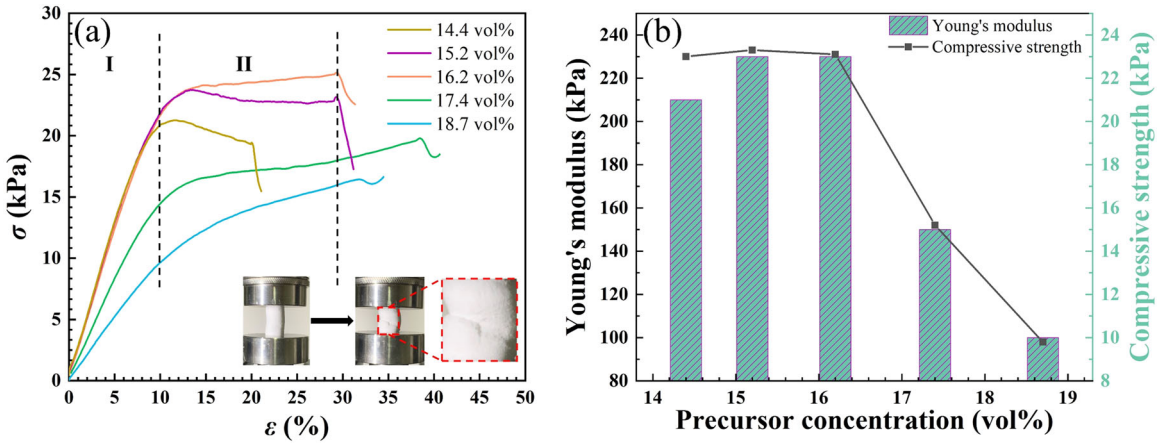

Fig. 9 **a** The σ–ε (stress-strain) curves, (**b**) the Young's modulus and the compressive strengths of MTES based aerogels with various precursor concentrations

3.6 Mechanical properties

Figure 9a shows the stress-strain (σ–ε) curves of different samples and the shape change during the uniaxial compression test. On the whole, the stress-strain curves can be roughly divided into two stages, I and II, which represent the elastic deformation stage and the plastic deformation stage, respectively. The turning point connecting stage I and II is just the yield point [58]. Obviously, the silica skeleton plays the crucial role of bearing external forces. In stage I ($\varepsilon < 10\%$), the three-dimensional silica skeletons are compressed by gathering together closer, and the pores are also compressed with the pore volume reducing. After the external force is removed, the compressed silica skeletons and pores begin to recover the original shape. The stage I indicates that the as-prepared MTES based aerogels have a nice elasticity at this stage. In stage II ($10\% < \varepsilon < 30\%$), the three-dimensional silica skeletons are compressed excessively with parts of the skeletons cracking and collapsing. As a consequence, the silica skeletons only can recover partly with remaining the permanent plastic deformation to some extent. The whole process is the elastic-plastic deformation and the MTES based aerogel in this study is a type of elastic-plastic material [58].

At the end of the stage II, the MTES based aerogels will fracture, indicating the material failure completely. It finds in the σ–ε curves that the material failure occurs earlier for the MTES based aerogel with 14.4 vol% precursor concentration when compared to others. It also finds that the larger precursor concentration indicates a later material failure. As analyzed in the microstructure section, more fractures are formed on the silica skeletons for the MTES based aerogel prepared with the lower precursor concentration, while the connectivity gets better for the MTES based aerogel prepared with the higher precursor concentration. The formed fractures act as the defects in the

MTES based aerogels and tend to induce material failure. Hence, it indicates that the microstructure characteristics are just consistent with the mechanical behavior as presented in Fig. 9a.

The changes of Young's modulus and compression strength are presented in Fig. 9b. Therein, Young's modulus keeps almost constant, about 230 kPa at precursor concentration below 16.2 vol%, and then decreases to 98 kPa with the precursor concentration increasing. The decreasing Young's modulus indicates that the MTES based aerogels with 18.7 and 17.4 vol% precursor concentrations are more flexible. Furthermore, the compressive strength has the same trend, i.e., decreasing from 23 kPa to 10 kPa.

At the lower precursor concentration (<16.2 vol%), the MTES based aerogels have slender backbones and the distribution of the skeletons is relatively denser, which can transfer the external force uniformly and avoid stress concentration. Although the existed fractures would induce the material failure earlier, the stronger ability to resist the deformation and bear the external force is achieved. Consequently, the larger Young's modulus and compressive strength are obtained. With the precursor concentration increasing (>16.2 vol%), the MTES based aerogels have thicker backbones and the distribution of the skeletons is relatively sparser. Despite the increase of the compressive strength for the single skeleton, a larger external force will concentrate on relatively fewer skeletons, and once exceed the compressive strength of the single skeleton, the material yield finally occurs. This microstructure leads to the lower Young's modulus and compressive strength. In sum, the mechanical properties of the MTES based aerogels primarily rely on their microstructure, which can influence the mechanical behavior by the corresponding skeleton density, skeleton diameter, and their connectivity.

4 Conclusions

In this study, the MTES based aerogels were prepared under ambient pressure by a facile synthesis approach using pure water as the only solvent. The effects of precursor concentration on the physicochemical properties of MTES based aerogels are studied in detail. The main conclusions are summarized as followed.

With the precursor concentration rising from 14.4 to 18.7 vol%, the silica skeletons of the prepared MTES based aerogels become stronger but sparser, making the bulk density increase from 0.057 g/cm^3 to 0.069 g/cm^3; the porosity shows a contrary tendency within 97.5–96.9%. The precursor concentration almost has no effect on the chemical composition, while it makes a great difference to the microstructure, i.e., the lower precursor concentration causing the denser and slenderer skeletons, vice versa. The microstructure further affects the mechanical properties of MTES based aerogel, and the slender and dense silica skeletons can effectively avoid stress concentration. From the perspective of the contact angle, the precursor concentration has no significant influence on the hydrophobicity of MTES based aerogels. In regard to the thermal property, the pores of MTES based aerogel are mainly micron-sized, which nearly do not contribute to the Knudsen effect. Due to the slender and dense skeletons, these MTES based aerogels have the higher thermal resistance, which leads to a lower solid thermal conductivity. Furthermore, the onset temperature of 425 °C indicates the good thermal stability of the as-prepared MTES based aerogels. From the view of preparation method, thermal conductivity, and thermal stability, these outcomes demonstrate the competitive advantages of the MTES based aerogels in the thermal insulation field.

Acknowledgements The authors deeply appreciate the supports from the National Natural Science Foundation of China (No. 51904336), the Natural Science Foundation of Hunan Province (No. 2020JJ4714), and the Fundamental Research Funds for the Central Universities (No. 202501003 and 202045001).

Compliance with ethical standards

Conflict of interest The authors declare no competing interests.

Publisher's note Springer Nature remains neutral with regard to jurisdictional claims in published maps and institutional affiliations.

References

1. Li Z, Cheng X, Gong L et al. (2018) Enhanced flame retardancy of hydrophobic silica aerogels by using sodium silicate as precursor and phosphoric acid as catalyst. J Non-Cryst Solids 481:267–275. https://doi.org/10.1016/j.jnoncrysol.2017.10.053
2. Pierre AC, Rigacci A (2011) SiO2 Aerogels. In: Aegerter MA, Leventis N, Koebel MM (eds) Aerogels Handbook. Springer New York, New York, NY, p 21–45
3. He F, Zhao H, Qu X et al. (2009) Modified aging process for silica aerogel. J Mater Process Technol 209:1621–1626. https://doi.org/10.1016/j.jmatprotec.2008.04.009
4. Wang Y, Li Z, Huber L et al. (2020) Reducing the thermal hazard of hydrophobic silica aerogels by using dimethyldichlorosilane as modifier. J Sol-Gel Sci Technol 93:111–122. https://doi.org/10.1007/s10971-019-05170-5
5. Randall JP, Meador MAB, Jana SC (2011) Tailoring mechanical properties of aerogels for aerospace applications. Acs Appl Mater Interfaces 3:613–626. https://doi.org/10.1021/am200007n
6. Li W, Willey RJ (1997) Stability of hydroxyl and methoxy surface groups on silica aerogels. J Non-Cryst Solids 212:243–249. https://doi.org/10.1016/S0022-3093(97)00021-5
7. Aegerter MA (2011) Aerogels Handbook. Springer New York, New York, NY
8. Omranpour H, Dourbash A, Motahari S (2014) Mechanical properties improvement of silica aerogel through aging: Role of

solvent type, time and temperature. Nuremberg, Germany 1593:298–302
9. Mahadik DB, Rao AV, Rao AP et al. (2011) Effect of concentration of trimethylchlorosilane (TMCS) and hexamethyldisilazane (HMDZ) silylating agents on surface free energy of silica aerogels. J Colloid Interface Sci 356:298–302. https://doi.org/10.1016/j.jcis.2010.12.088
10. Zhang W, Li Z, Shi L et al. (2019) Methyltrichlorosilane modified hydrophobic silica aerogels and their kinetic and thermodynamic behaviors: graphical Abstract. J Sol-Gel Sci Technol 89:448–457. https://doi.org/10.1007/s10971-018-4882-9
11. Smith D, Deshpande R, Brinke C (1992) Preparation of low-density aerogels at ambient pressure. MRS Proc 271:567–572. https://doi.org/10.1557/PROC-271-567
12. Soleimani Dorcheh A, Abbasi MH (2008) Silica aerogel; synthesis, properties and characterization. J Mater Process Technol 199:10–26. https://doi.org/10.1016/j.jmatprotec.2007.10.060
13. Koebel MM, Huber L, Zhao S, Malfait WJ (2016) Breakthroughs in cost-effective, scalable production of superinsulating, ambient-dried silica aerogel and silica-biopolymer hybrid aerogels: from laboratory to pilot scale. J Sol-Gel Sci Technol 79:308–318. https://doi.org/10.1007/s10971-016-4012-5
14. Huber L, Zhao S, Malfait WJ et al. (2017) Fast and minimal-solvent production of superinsulating silica aerogel granulate. Angew Chem Int Ed 56:4753–4756. https://doi.org/10.1002/anie.201700836
15. El Rassy H, Buisson P, Bouali B et al. (2003) Surface characterization of silica aerogels with different proportions of hydrophobic groups, dried by the CO2 supercritical method. Langmuir 19:358–363. https://doi.org/10.1021/la020637r
16. Dong H, Brennan JD (2006) Macroporous monolithic methylsilsesquioxanes prepared by a two-step acid/acid processing method. Chem Mater 18:4176–4182. https://doi.org/10.1021/cm060509e
17. Rao AV, Kulkarni MM, Amalnerkar DP, Seth T (2003) Superhydrophobic silica aerogels based on methyltrimethoxysilane precursor. J Non-Cryst Solids 330:187–195. https://doi.org/10.1016/j.jnoncrysol.2003.08.048
18. Xu B, Cai JY, Finn N, Cai Z (2012) An improved method for preparing monolithic aerogels based on methyltrimethoxysilane at ambient pressure Part I: Process development and macrostructures of the aerogels. Microporous Mesoporous Mater 148:145–151. https://doi.org/10.1016/j.micromeso.2011.08.012
19. Xu B, Cai JY, Xie Z et al. (2012) An improved method for preparing monolithic aerogels based on methyltrimethoxysilane at ambient pressure Part II: Microstructure and performance of the aerogels. Microporous Mesoporous Mater 148:152–158. https://doi.org/10.1016/j.micromeso.2011.08.015
20. He S, Chen X (2017) Flexible silica aerogel based on methyltrimethoxysilane with improved mechanical property. J Non-Cryst Solids 463:6–11. https://doi.org/10.1016/j.jnoncrysol.2017.02.014
21. Nadargi DY, Rao AV (2009) Methyltriethoxysilane: New precursor for synthesizing silica aerogels. J Alloy Compd 467:397–404. https://doi.org/10.1016/j.jallcom.2007.12.019
22. Nadargi DY, Latthe SS, Hirashima H, Rao AV (2009) Studies on rheological properties of methyltriethoxysilane (MTES) based flexible superhydrophobic silica aerogels. Microporous Mesoporous Mater 117:617–626. https://doi.org/10.1016/j.micromeso.2008.08.025
23. Aravind PR, Soraru GD (2011) High surface area methyltriethoxysilane-derived aerogels by ambient pressure drying. J Porous Mater 18:159–165. https://doi.org/10.1007/s10934-010-9366-4
24. Niu Z, He X, Huang T et al. (2019) A facile preparation of transparent methyltriethoxysilane based silica xerogel monoliths at ambient pressure drying. Microporous Mesoporous Mater 286:98–104. https://doi.org/10.1016/j.micromeso.2019.05.036
25. Shao Z, He X, Cheng X, Zhang Y (2017) A simple facile preparation of methyltriethoxysilane based flexible silica aerogel monoliths. Mater Lett 204:93–96. https://doi.org/10.1016/j.matlet.2017.05.104
26. Michel D (2018) Test of the formal basis of Arrhenius law with heat capacities. Phys Stat Mech Its Appl 510:188–199. https://doi.org/10.1016/j.physa.2018.06.125
27. Luo Y, Li Z, Zhang W et al. (2019) Rapid synthesis and characterization of ambient pressure dried monolithic silica aerogels in ethanol/water co-solvent system. J Non-Cryst Solids 503–504:214–223. https://doi.org/10.1016/j.jnoncrysol.2018.09.049
28. Barrett EP, Joyner LG, Halenda PP (1951) The determination of pore volume and area distributions in porous substances. I. Computations from nitrogen isotherms. J Am Chem Soc 73:373–380. https://doi.org/10.1021/ja01145a126
29. Kumar A, Verma SK, Alvi PA, Jasrotia D (2012) NIH Image to ImageJ: 25 years of image analysis. Nat Methods 9:671–675
30. Yun S, Guo T, Zhang J et al. (2017) Facile synthesis of large-sized monolithic methyltrimethoxysilane-based silica aerogel via ambient pressure drying. J Sol-Gel Sci Technol 83:53–63. https://doi.org/10.1007/s10971-017-4377-0
31. Rojas F, Kornhauser I, Felipe C et al. (2002) Capillary condensation in heterogeneous mesoporous networks consisting of variable connectivity and pore-size correlation. Phys Chem Chem Phys 4:2346–2355. https://doi.org/10.1039/b108785a
32. Zhi L, Cheng X, Song H et al. (2016) Aramid fibers reinforced silica aerogel composites with low thermal conductivity and improved mechanical performance. Compos Part Appl Sci Manuf 84:316–325
33. Li Z, Zhao S, Koebel MM, Malfait WJ (2020) Silica aerogels with tailored chemical functionality. Mater Des 193:108833. https://doi.org/10.1016/j.matdes.2020.108833
34. Cheng X, Li C, Shi X et al. (2017) Rapid synthesis of ambient pressure dried monolithic silica aerogels using water as the only solvent. Mater Lett 204:157–160. https://doi.org/10.1016/j.matlet.2017.05.107
35. Lin YF, Hsu SH (2017) Solvent-resistant CTAB-modified polymethylsilsesquioxane aerogels for organic solvent and oil adsorption. J Colloid Interface Ence 485:152–158
36. Mahadik DB, Rao AV, Parale VG et al. (2011) Effect of surface composition and roughness on the apparent surface free energy of silica aerogel materials. Appl Phys Lett 99:104
37. Socrates G, Socrates G (2001) Infrared and Raman characteristic group frequencies: tables and charts, 3rd ed. Wiley, Chichester; New York, NY
38. Al-Oweini R, El-Rassy H (2009) Synthesis and characterization by FTIR spectroscopy of silica aerogels prepared using several Si(OR)4 and R″Si(OR′)3 precursors. J Mol Struct 919:140–145
39. Li Z, Cheng X, He S et al. (2015) Characteristics of ambient-pressure-dried aerogels synthesized via different surface modification methods. J Sol-Gel Sci Technol 76:138–149. https://doi.org/10.1007/s10971-015-3760-y
40. Pan Y, He S, Gong L et al. (2017) Low thermal-conductivity and high thermal stable silica aerogel based on MTMS/Water-glass co-precursor prepared by freeze drying. Mater Des 113:246–253. https://doi.org/10.1016/j.matdes.2016.09.083
41. Wu X, Li Z, Joao G et al. (2020) Reducing the flammability of hydrophobic silica aerogels by tailored heat treatment. J Nanopart Res 22:1–16. https://doi.org/10.1007/s11051-020-04822-w
42. Huang S, Wu X, Li Z et al. (2020) Rapid synthesis and characterization of monolithic ambient pressure dried MTMS aerogels in pure water. J Porous Mater 27:1241–1251. https://doi.org/10.1007/s10934-020-00902-3
43. Matias T, Varino C, de Sousa HC et al. (2016) Novel flexible, hybrid aerogels with vinyl- and methyltrimethoxysilane in the

underlying silica structure. J Mater Ence 51:6781–6792. https://doi.org/10.1007/s10853-016-9965-9
44. Li Z, Cheng X, He S (2016) Tailoring thermal properties of ambient pressure dried MTMS/TEOS co-precursor aerogels. Mater Lett 171:91–94. https://doi.org/10.1016/j.matlet.2016.02.025
45. Lu X, Arduini-Schuster MC, Kuhn J et al. (1992) Thermal conductivity of monolithic organic aerogels. SCIENCE 255:971–2. https://doi.org/10.1126/science.255.5047.971
46. Koebel M, Rigacci A, Achard P (2012) Aerogel-based thermal superinsulation: an overview. J Sol-Gel Sci Technol 63:315–339. https://doi.org/10.1007/s10971-012-2792-9
47. Lee OJ, Lee KH, Yim TJ et al. (2002) Determination of mesopore size of aerogels from thermal conductivity measurements. J Non-Cryst Solids 298:287–292. https://doi.org/10.1016/S0022-3093(01)01041-9
48. Groult S, Budtova T (2018) Thermal conductivity/structure correlations in thermal super-insulating pectin aerogels. Carbohydr Polym 196:73–81. https://doi.org/10.1016/j.carbpol.2018.05.026
49. Li CH, Jiang SC, Yao ZP et al. (2014) Research on heat transfer characteristics of nano-porous silica aerogel material and its application on mars surface mission. Adv Mater Res 924:329–335. https://doi.org/10.4028/www.scientific.net/AMR.924.329
50. Li Z, Zhang Y, Huang S et al. (2020) Thermal stability and pyrolysis characteristics of MTMS aerogels prepared in pure water. J Nanopart Res 22:334. https://doi.org/10.1007/s11051-020-05062-8
51. Huang D, Guo C, Zhang M, Shi L (2017) Characteristics of nanoporous silica aerogel under high temperature from 950 °C to 1200 °C. Mater Des 129:82–90. https://doi.org/10.1016/j.matdes.2017.05.024
52. Li C, Cheng X, Li Z et al. (2017) Mechanical, thermal and flammability properties of glass fiber film/silica aerogel composites. J Non-Cryst Solids 457:52–59. https://doi.org/10.1016/j.jnoncrysol.2016.11.017
53. Li Z, Cheng X, Shi L et al. (2016) Flammability and oxidation kinetics of hydrophobic silica aerogels. J Hazard Mater 320:350–358. https://doi.org/10.1016/j.jhazmat.2016.07.054
54. Rao AV, Kulkarni MM, Amalnerkar DP, Seth T (2003) Surface chemical modification of silica aerogels using various alkylalkoxy/chloro silanes. Appl Surf Sci 206:262–270. https://doi.org/10.1016/S0169-4332(02)01232-1
55. Li Z, Huang S, Shi L et al. (2019) Reducing the flammability of hydrophobic silica aerogels by doping with hydroxides. J Hazard Mater 373:536–546. https://doi.org/10.1016/j.jhazmat.2019.03.112
56. He S, Huang Y, Chen G et al. (2019) Effect of heat treatment on hydrophobic silica aerogel. J Hazard Mater 362:294–302. https://doi.org/10.1016/j.jhazmat.2018.08.087
57. He S, Huang D, Bi H et al. (2015) Synthesis and characterization of silica aerogels dried under ambient pressure bed on water glass. J Non-Cryst Solids 410:58–64. https://doi.org/10.1016/j.jnoncrysol.2014.12.011
58. James MG, Barry JG (1997) Mechanics of Materials, 7 th. Cengage, Canada
59. Wagh PB, Begag R, Pajonk GM et al. (1999) Comparison of some physical properties of silica aerogel monoliths synthesized by different precursors. Mater Chem Phys 57:214–218. https://doi.org/10.1016/S0254-0584(98)00217-X
60. Liu GW, Ni XY, Zhou B, Yu QJ (2012) Preparation and characterization of ultralow density silica aerogels by acetonitrile supercritical drying. Key Eng Mater 519:83–86
61. Gauthier BM, Bakrania SD, Anderson AM, Carroll MK (2004) A fast supercritical extraction technique for aerogel fabrication. J Non-Cryst Solids 350:238–243. https://doi.org/10.1016/j.jnoncrysol.2004.06.044
62. Zhang Y, Peng et al. (2016) An economic and environmentally benign approach for the preparation of monolithic silica aerogels. RSC Adv 6:1–11. https://doi.org/10.1039/C6RA21050C
63. Bisson A, Rigacci A, Lecomte D, Achard P (2004) Effective thermal conductivity of divided silica xerogel beds. J Non-Cryst Solids 350:379–384. https://doi.org/10.1016/j.jnoncrysol.2004.08.238
64. Li Z, Gong L, Li C et al. (2016) Silica aerogel/aramid pulp composites with improved mechanical and thermal properties. J Non-Cryst Solids 454:1–7. https://doi.org/10.1016/j.jnoncrysol.2016.10.015
65. Lee SE, Ahn YS, Lee JS et al. (2017) Ambient-pressure drying synthesis of high-performance silica aerogel powders by controlling hydrolysis reaction of water glass. J Ceram Process Res 18:777–782
66. Li Z, Cheng X, Gong L et al. (2017) Enhanced flame retardancy of hydrophobic silica aerogels by using sodium silicate as precursor and phosphoric acid as catalyst. J Non-Cryst Solids 481:267–275. https://doi.org/10.1016/j.jnoncrysol.2017.10.053
67. Hegde ND, Venkateswara Rao A (2007) Physical properties of methyltrimethoxysilane based elastic silica aerogels prepared by the two-stage sol–gel process. J Mater Sci 42:6965–6971. https://doi.org/10.1007/s10853-006-1409-5